DMD Fast Forward. Published on December 7, 2010 as doi:10.1124/dmd.110.036723
This article has not been copyedited and formatted. The final version may differ from this version.

Identification of 20(*S*)-Protopanaxadiol Metabolites in Human Liver Microsomes and Human Hepatocytes

Liang Li, Xiaoyan Chen, Dan Li and Dafang Zhong

Shanghai Institute of Materia Medica, Chinese Academy of Sciences, Shanghai, China (L. L., X. C., D. L., D. Z.)

Running Title

20(*S*)-Protopanaxadiol Metabolite Identification

Corresponding Author: Dafang Zhong

Shanghai Institute of Materia Medica, Chinese Academy of Sciences, 501 Haike Road, Shanghai 201203, China

Phone: 0086-21-50800738

Fax: 0086-21-50800738

Email: dfzhong@mail.shcnc.ac.cn

Number of text pages: 28 (Without Refs)

Number of tables: 2

Number of figures: 9

Number of references: 25

Number of words in the Abstract: 222

Number of words in the Introduction: 377

Number of words in the Discussion: 1081

Abbreviations: PPD, 20(*S*)-protopanaxadiol; PPT, 20(*S*)-protopanaxatriol; 5-HT, 5-hydroxytryptamine; HSQC, heteronuclear multiple quantum coherence; COSY, correlation spectroscopy; HMBC, heteronuclear multiple-bond correlation; NOESY, nuclear Overhauser enhancement spectroscopy; LC/MS^n, liquid chromatography/ion trap mass spectrometry; EIC,

extracted ion chromatogram; ESI, electrospray ionization; *m*-CPBA, 3-chloroperoxybenzoic acid; HLMs, human liver microsomes.

Abstract

20(*S*)-Protopanaxadiol (PPD, **1**, Fig. 1) is one of the aglycones of the ginsenosides and has a wide range of pharmacologic activities. Currently, PPD has progressed to early clinical antidepressant trials. In this study, its fate in mixed human liver microsomes (HLMs) and human hepatocytes were examined for the first time. Using of liquid chromatography-electrospray ionization ion trap mass spectrometry (LC/MS^n), 24 metabolites were found. Four metabolites were isolated, and their structures were elucidated as (20*S*,24*S*)-epoxydammarane-3,12,25-triol (**2**), (20*S*,24*R*)-epoxy-dammarane-3,12,25-triol (**3**), (20*S*,24*S*)-epoxydammarane-12,25-diol-3-one (**4**), and (20*S*,24*R*)-epoxydammarane-12,25-diol-3-one (**5**) based on a detailed analysis of their spectroscopic data. The predominant metabolic pathway of PPD observed was the oxidation of the 24,25-double bond to yield 24,25-epoxides, followed by hydrolysis and rearrangement to form the corresponding 24,25-vicinal diol derivatives (M6) and the 20,24-oxide form (**2** and **3**). Further sequential metabolites (M2–M5) were also detected through the hydroxylation and dehydrogenation of **2** and **3**. All of the Phase I metabolites except for M1-1 possess a hydroxyl group at C-25 of the side chain, which was newly formed by biotransformation. Two glucuronide conjugates (M7) attribute to **2** and **3** were detected in human hepatocyte incubations, and the conjugation sites of them were tentatively assigned to the 25-hydroxyl group. The findings of this paper strongly suggested that the formation of the 25-hydroxyl group is very important for the elimination of PPD.

Introduction

Ginseng, one of the most famous medicinal herbs, has been used widely in Asia, Europe, and North America. The major pharmacologically active components of ginseng are ginsenosides, a diverse group of steroidal saponins that target multitudinous tissues, producing an array of pharmacological responses (Lee et al., 2005a; Park et al., 2004; Kim et al., 2003). The most abundant ginsenosides can be subdivided into two classes based on the aglycones: 20(*S*)-protopanaxadiol (PPD) type and 20(*S*)-protopanaxatriol (PPT) type (Shibata et al., 1966; Tanaka et al., 1966).

PPD is one of the aglycones of the ginsenosides. This compound has a wide range of pharmacologic activities, including those that are anti-estrogenic (Yu et al., 2007; Leung et al., 2009), anti-inflammatory (Lee et al., 2005b; Lee et al., 2006), antitumor (Zhang et al., 2008; Li et al., 2006; Popovich et al., 2004; Liu et al., 2007; Usami et al., 2008), vasodilator (Chang et al., 1994), and anti-nociceptive (Shin et al., 1997). It has been found to have inhibitory effects on CYP3A activity (Liu et al., 2004; Liu et al., 2006). Hui et al. (2006) have reported that PPD markedly increases the levels of norepinephrine and 5-hydroxytryptamine (5-HT) in the brain of rats with symptoms of depression, and significantly enhances the tremor effect of 5-HT (Hui et al., 2006). Currently, PPD has progressed to early clinical antidepressant trials.

Our previous experiment shows that its oral bioavailability is low (rats: 31%, 25 mg/kg; dogs: 9.6%, 8 mg/kg) due to its extensive metabolism in the gastrointestinal tract. Kasai et al. have found that incubation of PPD with microsomes from rat livers has led to the formation of its 20,24-oxides as major metabolites (Kasai et al., 2000). By comparison of FAB-MS, EI-MS and retention time of HPLC with those of authentic samples derived from PPD by oxidation with 3-chloroperoxybenzoic acid, the formation of (20*S*,24*S*)-epoxydammarane-3,12,25-triol (**2**) was confirmed. Due to overlaps

with other minor peaks in the HPLC, the formation of (20*S*,24*R*)-epoxydammarane-3,12,25-triol (**3**) was ambiguous. Remarkably, there have been no reports of its metabolism in humans. In this study, its fate in HLMs and human hepatocytes were examined by means of LC/MS^n. The objective of this study was to gain understanding about the whole metabolic route of PPD in humans including the biotransformation to the 24,25-epoxide metabolites.

Materials and Methods

Chemicals. 20(*S*)-Protopanaxadiol was kindly provided by the Shanghai Innovative Research Center of Traditional Chinese Medicine (Shanghai, China). Pooled human liver microsomes were purchased from BD Gentest (Woburn, MA, USA). NADPH, UDP-glucuronic acid (UDPGA) and alamethicin were purchased from Sigma-Aldrich (St. Louis, MO, USA). Cryopreserved human hepatocytes were purchased from the Research Institute for Liver Diseases (Shanghai) Co., LTD (Shanghai, China). All solvents used for high performance liquid chromatography (HPLC) and ultrahigh performance liquid chromatography with quadrupole time of flight mass spectrometry (UPLC/Q-TOF MS) were of HPLC grade (Merck, Darmstadt, Germany). All solvents used for gel chromatography and $MgCl_2$ were of analytical grade (Shanghai Chemical Plant, Shanghai, China). Silica gel (300–400 mesh, Qingdao Marine Chemical Plant, Qingdao, China), Sephadex LH-20 gel (Amersham Biosciences, Uppsala, Sweden) and C18 reversed-phase silica gel (150–200 mesh, Merck, Darmstadt, Germany) were used for column chromatography, and pre-coated silica gel GF254 plates (Qingdao Marine Chemical Plant, Qingdao, China) were used for thin-layer chromatography (TLC). 3-Chloroperoxybenzoic acid (*m*-CPBA) was purchased from Alfa Aesar China (Tianjin) Co., Ltd.

Microsomal Incubations of PPD and the Isolated Metabolites. All incubations were performed at 37°C in a water bath shaker. Stock solution of PPD was prepared in MeOH. The final concentration of MeOH in the incubation was 0.1% (v/v). The pooled human liver microsomes (HLMs) were carefully thawed on ice prior to the experiment. HLM proteins (1.0 mg/ml) were added to a solution of PPD (50 μM) in 100 mM potassium phosphate buffer (pH 7.4). The total incubation volume was 200 μl. After 3 min of preincubation at 37°C, the incubation reactions were initiated by the addition of NADPH (2.0 mM). After undergoing incubation for 60 min, the reactions were terminated with an equal

volume of ice-cold acetonitrile. Control samples containing no NADPH or substrates were included; each incubation was performed in duplicate. All incubation conditions for the isolated metabolites **2**, **3**, **4** and **5** were the same as described above for PPD.

Incubation of PPD with Human Hepatocytes. Stock solution of PPD was prepared in MeOH. The final concentration of MeOH in the incubation was 0.5% (v/v). All the incubations were conducted at 37°C for 3 h in Williams' E medium containing PPD (50 μM) and hepatocytes (2 million cells/ml). Incubations in the presence of PPD at time 0 h or in the absence of PPD at 3 h served as negative controls. Reactions were quenched with an equal volumes of acetonitrile, each incubation was performed in duplicate.

Microsomal Incubations of PPD, 2 and 3 with the Presence of UDPGA. All incubations were performed at 37°C in a water bath shaker. Stock solution of the PPD was prepared in MeOH. The final concentration of MeOH in the incubation was 0.1% (v/v). The pooled human liver microsomes (HLMs) were carefully thawed on ice prior to the experiment. HLM proteins (1.0 mg/ml) were added to a solution of 10 mM $MgCl_2$, 2 mM UDP-glucuronic acid (UDPGA) and 25 μg/mL alamethicin in 50 mM Tris–HCl buffer (pH 7.4). The total incubation volume was 200 μl. After 3 min of preincubation at 37°C, the incubation reactions were initiated by the addition of PPD (50 μM). After undergoing incubation for 120 min, the reactions were terminated with an equal volume of ice-cold acetonitrile. Incubations in the presence of PPD at time 0 min served as negative controls, each incubation was performed in duplicate. The incubation conditions for **2** and **3** were the same as described above for PPD.

Preparation of Samples for LC/MS^n Analysis. All the *in vitro* incubation samples were prepared by the same methods as follows: to a 200 μl aliquot of the *in vitro* incubations, 200 μl of methanol was

added. This sample was vortex-mixed and centrifuged at 14,000*g* for 5 min. The supernatant was transferred into a glass tube, evaporated to dryness under a stream of nitrogen at 40°C, and then reconstituted in 100 μl of 0.1% formic acid in methanol with 0.1% formic acid in 5 mM ammonium acetate (70: 30, v/v). A 20 μl aliquot of the reconstituted solution was injected into the LC/MS^n system for analysis.

Oxidation of PPD with *m*-CPBA. A solution of PPD (100 μM) and *m*-CPBA (10 μM) in CH_2Cl_2 (5 ml) was stirred at room temperature for 15 and 60 minutes. The reaction mixtures were poured into Na_2CO_3 saturated ice water and extracted three times with ether. The ether extracts were evaporated to dryness under a vacuum, and then reconstituted in 5 ml of 0.1% formic acid in methanol with 0.1% formic acid in 5 mM ammonium acetate (70: 30, v/v). A 20 μl aliquot of the reconstituted solution was injected into the LC/MS^n system for analysis.

Experimental Animals. The rat studies were conducted according to protocols approved by the Review Committee of Animal Care and Use at the Shanghai Institute of Materia Medica (Shanghai, China). Male Sprague-Dawley rats (200–250 g; Shanghai SLAC Laboratory Animal Co., Shanghai, China) were housed in rat cages. Filtered tap water was available *ad libitum*, and the rodents were given commercial rat pellets *ad libitum* except for the overnight period before dosing. The rats were acclimated to the facilities and the environment 2 days prior to the experiments.

Feces Sample Collection. For oral administration, PPD was prepared as 10 mg/ml solution in 0.5% carboxymethyl cellulose sodium salt, 0.5% polysorbate-80 and 99% saline. The solution was stirred at room terperature pending use. In all, 20 rats were housed in Nalgene metabolic cages (1 rat per cage) and given continuous oral PPD at 100 mg/kg/day (via gavage, once-daily) for 11 days. The PPD feces samples were collected within a period of 0–288 h. The blank feces samples were collected prior to

DMD Fast Forward. Published on December 7, 2010 as DOI: 10.1124/dmd.110.036723
This article has not been copyedited and formatted. The final version may differ from this version.

dosing. The feces samples were frozen at –20°C immediately after collection.

NMR Instrument. NMR spectra (^{1}H and ^{13}C NMR, distorsionless enhancement by polarization transfer, ^{1}H-^{1}H COSY, HSQC, HMBC, and NOESY) were recorded on an Varian Mercury 400 spectrometer (400 MHz for ^{1}H and 100 MHz for ^{13}C), and chemical shifts were recorded in parts per million using tetramethylsilane as an internal standard. Deuterium chloroform ($CDCl_3$) was used as a solvent for all of the metabolites.

Chromatography. The Agilent 1200 HPLC was equipped with a reversed-phase column (Eclipse XDB-C8, 4.6 mm × 150 mm i.d., 5 μm, Agilent, USA) protected by a 4.0 mm × 3.0 mm i.d. Security Guard (5 μm) C18 guard column (Phenomenex, Torrance, CA, USA). The mobile phase was a mixture of (A) 0.1% formic acid in methanol and (B) 0.1% formic acid in 5 mM ammonium acetate with gradients programmed as follows: initial 70% A maintained for 3 min, which was increased to 100% in 17 min maintained for 5 min, and then finally decreased to 70% A in 0.1 min maintained for 10 min. The flow rate was 0.5 ml/min, and the injection volume was 20 μl.

The Ion Trap Mass Spectrometer. The LC/MS^n experiment was carried out on an Agilent 6330 LC/MSD Trap XCT ultra (Agilent Technologies, Waldbronn, Germany). The mass spectrometer (MSD) was equipped with an ESI source. The ionization mode was positive. The interface and MSD parameters were as follows: nebulizer pressure 40 psi (N_2), dry gas 12 ml/min (N_2), dry gas temperature 350°C, spray capillary voltage 3500 V, skimmer voltage 40 V, ion transfer capillary exit 124 V, scan range *m*/*z* 100–800, spectra average 3, and dwell time 200 ms. For the MS^n spectra, the fragmentation amplitude varied between 0.4 and 0.9 V. Other parameters, including the potential of the octapole offset and that of the tube lens offset, were also optimized for maximum abundance of the ions of interest by the automatic tune feature of the instrument. The MS^n product-ion spectra were

DMD Fast Forward. Published on December 7, 2010 as DOI: 10.1124/dmd.110.036723
This article has not been copyedited and formatted. The final version may differ from this version.

produced by collision-induced dissociation of the molecular ions $[M + H]^+$ of all analytes at their respective HPLC retention times. Data acquisition was performed in full-scan LC/MS and MS^n modes. All data acquired were processed by Agilent Chemstation Rev. B. 01.03 software (Agilent, Palo Alto, CA, USA).

UPLC Conditions. Chromatographic separation was performed using a Waters ACQUITY UPLC system equipped with a binary solvent delivery system, column oven, and autosampler. Chromatographic separations were achieved on a reversed-phase column (Eclipse XDB-C8, 4.6 mm × 150 mm i.d., 5 μm, Agilent, USA) protected by a 4.0 mm × 3.0 mm i.d. Security Guard (5 μm) C18 guard column (Phenomenex, Torrance, CA, USA). Thermostated at 35°C, the autosampler was maintained at 10°C. The mobile phase was a mixture of 87% A (0.1% formic acid in methanol) and 13% B (0.1% formic acid in 5 mM ammonium acetate), the flow rate was 0.5 ml/min, and the injection volume was 10 μl (10 μg/ml in MeOH).

The Q-TOF MS Conditions. The high mass resolution experiments were carried out on a Synapt™ Q-TOF mass spectrometer (Waters Corp., Milford, MA, USA) equipped with an ESI source in positive ion mode. The capillary and cone voltages were 2000 V and 40 V, respectively. The desolvation gas (nitrogen) was set to 700 l/h at a temperature of 350°C, and the source temperature was 120°C. Data were acquired from 100 to 600 Da and corrected during acquisition using an external reference (lock spray) composed of a solution of 600 ng/ml leucine enkephalin (*m/z* 566.2771) infused at 5 μl/min. The transfer collision energy (CE) and trap CE were 4 and 6 eV to acquire MS data; while the transfer CE was 15 eV and the trap CE were ramped from 20 to 30 eV to acquire MS/MS data. The raw data were acquired and processed by the Masslynx™ Version 4.1 (Waters Corp., Milford, MA, USA).

DMD Fast Forward. Published on December 7, 2010 as DOI: 10.1124/dmd.110.036723
This article has not been copyedited and formatted. The final version may differ from this version.

Isolation of the Metabolites. The rat feces (1.4 kg) were extracted exhaustively with MeOH (6.0 l) at room temperature. The methanolic extract was evaporated to give a residue, which was partitioned between EtOAc and H_2O. The EtOAc-soluble portion (24.5 g) was subjected to column chromatography on silica gel using 20%→100% EtOAc in petroleum ether (PE) as eluent to produce 5 fractions (A–E) based on TLC checking. Fraction B (2.1 g) was chromatographed over a column of Sephadex LH-20 eluted with MeOH, followed by C18 reversed-phase silica gel eluted with MeOH/H_2O 92:8 to give **5** (7.8 mg). Fraction C (1.7 g) was purified by column chromatography (Sephadex LH-20, MeOH) to yield 3 sub-fractions (C1–C3). Fraction C2 was further chromatographed over a column of C18 reversed-phase silica gel eluted with MeOH/H_2O 90:10 to obtain **3** (41.5 mg). Fraction D (4.1 g) was chromatographed over a column of Sephadex LH-20 eluted with MeOH, followed by C18 reversed-phase silica gel eluted with MeOH/H_2O gradient (from 85:15—95:5) to give **2** (94.6 mg) and **4** (11.5 mg).

Results

Mass Spectral Properties of PPD. Proper metabolite identification using the LC/MS^n approach requires a comprehensive understanding of the fragmentation behavior of the parent compound to be tested. Given the presence of three hydroxyl groups in the molecule, PPD is prone to generate in-source dissociation fragment ions under a higher source temperture. At a source temperature lower than 250°C, the parent ion at *m*/*z* 461 can be detected. However, the mass spectral response of PPD and its metabolites decreased dramatically, we choose a source temperature of 350°C to carried out experiments. Under the experimental conditions, the protonated molecule of PPD (*m/z* 461) was not detected under positive scan mode (Fig. 2). The LC peak at 22.3 min retention time showed typical in-source dissociation fragment ions at *m/z* 443 ($[M + H - H_2O]^+$), 425 ($[M + H - 2H_2O]^+$) and 407 ($[M + H - 3H_2O]^+$), as well as adduct ions at *m/z* 483 ($[M + Na]^+$).

Structure Elucidation of PPD Metabolites in HLMs. Fig. 3 shows the total ion and extracted ion chromatograms of the parent drug and its metabolites after 60 min of incubation with HLMs. Compared with the blank sample, 20 metabolites were observed.

These metabolites may be mainly classified into 5 types: M1 (*m*/*z* 477) from the metabolic addition of one oxygen atom (+ 16 from the parent), M2 (*m*/*z* 475) from the addition of an oxygen atom with dehydrogenation (+ 14 from the parent), M3 (*m*/*z* 491) from the addition of 2 oxygen atoms with dehydrogenation (+ 30 from the parent), M4 (*m*/*z* 493) from the addition of 2 oxygen atoms (+ 32 from the parent), and M5 (*m*/*z* 509) from the addition of 3 oxygen atoms (+ 48 from the parent). These metabolites were numbered according to their chromatographic retention times, and the structures were elucidated through their mass spectral fragments.

Metabolite M1. In the HLMs incubations, M1-1, M1-2, and M1-3 were detected at 18.7, 19.2 and 19.8

min, respectively, with a protonated molecular weight of 477 (*m/z* 461 + 16), which indicates the addition of one oxygen atom into the molecule. The MS^2 spectra (Fig. 4A) showed identical fragment ions at *m/z* 459 (– 18), 441 (– 36), 423 (– 54), 405 (– 72), 191, and 143. The fragment ion of *m/z* 143 was attributed to the oxidation of the side chain, suggesting that the + 16 modification occurred on the side chain moiety. By comparing the chromatographic retention times and mass spectral fragmentation patterns with the isolated metabolites, M1-2 and M1-3 were confirmed as the (20*S*,24*S*)-epoxydammarane-3,12,25-triol (**2**) and (20*S*,24*R*)- epoxydammarane-3,12,25-triol (**3**), respectively.

***Metabolite M2*.** M2 was detected with a protonated molecular weight of 475, which was 14 Da higher than the protonated parent drug, indicating the introduction of an oxygen atom with dehydrogenation. M2-1 and M2-2 were detected at 19.1 and 19.7 min, respectively, in the HLMs incubations. The MS^2 spectra (Fig. 4B) showed fragment ions at *m/z* 457 (– 18), 439 (– 36), 421 (– 54) and 143. The fragment ion of *m/z* 143 indicated that the + 16 modification occurred on the side chain moiety, and the absence of the fragment ion of *m/z* 191 indicated that the dehydrogenation was occurred at C-3. The chromatographic retention time and mass spectral fragmentation patterns of M2-1 and M2-2 were identical to the isolated metabolites (20*S*,24*S*)-epoxydammarane-12,25-diol-3-one (**4**) and (20*S*,24*R*)-epoxy dammarane- 12,25-diol-3-one (**5**), respectively. M2-1 and M2-2 were accordingly confirmed as (20*S*,24*S*)- epoxydammarane-12,25-diol-3-one and (20*S*,24*R*)-epoxydammarane-12,25-diol-3-one, respectively.

***Metabolite M3*.** M3 was detected with a protonated molecular weight of 491, which was 30 Da higher than the protonated parent drug, indicating the introduction of 2 oxygen atoms with dehydrogenation. Up to 6 independent chromatographic peaks with protonated ions at *m/z* 491 were detected in the

HLMs incubations.

Metabolites M3-1, M3-3, and M3-4 were detected at 11.9, 14.8 and 15.3 min, respectively. The MS^2 spectra (Fig. 4C) showed fragment ions at *m/z* 473 (– 18), 455 (– 36), 437 (– 54), 419 (– 72), 191 and 143. M3-1, M3-3, and M3-4 were tentatively identified as the dioxygenation and dehydrogenation products of PPD. One of the oxygen atoms was introduced into the side chain of the molecule. The position of the other oxygen and the dehydrogenation were unclear.

Metabolite M3-2, was detected at 14.0 min. The MS^2 spectra (Fig. 4D) showed fragment ions at *m/z* 473 (– 18), 455 (– 36), 437 (– 54), 419 (– 72) and 143. M3-2 was tentatively identified as the dioxygenation and dehydrogenation products of PPD. One of the oxygen atoms was introduced into the side chain of the molecule. The position of the other oxygen was unclear. Furthermore, The absence of the fragment ion of *m/z* 191 indicated that the dehydrogenation was occurred at C-3.

Metabolite M3-5 was detected at 17.4 min. The MS^2 spectra (Fig. 4E) showed major fragment ions at *m/z* 473 (– 18), 455 (– 36), 437 (– 54), 419 (– 72), 159, and 141. The fragment ion of *m/z* 159 was attributed to the dioxygenation of the side chain. This suggests that the + 32 modification both occurred at the side chain. M3-5 was identified as the dioxygenation and dehydrogenation product of PPD, and both of the oxygen atoms were introduced into the side chain of the molecule. Furthermore, The absence of the fragment ion of *m/z* 191 also indicated that the dehydrogenation was occurred at C-3.

Metabolite M3-6 was detected at 18.9 min. The MS^2 spectra (Fig. 4F) showed major fragment ions at *m/z* 473 (– 18), 455 (– 36), 191, and 157. The fragment ion at *m/z* 157 indicated that all of the modifications took place at the side chain. Thus, M3-6 was confirmed as the side chain dioxygenation and dehydrogenation product of PPD.

DMD Fast Forward. Published on December 7, 2010 as DOI: 10.1124/dmd.110.036723
This article has not been copyedited and formatted. The final version may differ from this version.

***Metabolite M4*.** M4 was detected with a protonated molecular weight of 493, which was 32 Da higher than the protonated PPD, indicating the introduction of 2 oxygen atoms. In addition, 5 independent chromatographic peaks with protonated ions at *m/z* 493 were detected in the HLMs incubations.

Metabolites M4-1, M4-2, and M4-3 were detected at 11.3, 14.4 and 15.4 min, respectively. The MS^2 spectra (Fig. 4G) showed fragment ions at *m/z* 475 (– 18), 457 (– 36), 439 (– 54), 421 (– 72), 191 and 143. M4-1, M4-2, and M4-3 were identified as the dioxygenation products of PPD, with one of the oxygen atoms introduced into the side chain of the molecule. The position of the other oxygen was unclear.

M4-4 and M4-5 were detected at 17.0 and 17.8 min, respectively. The MS^2 spectra (Fig. 4H) showed major fragment ions at *m/z* 475 (– 18), 457 (– 36), 439 (– 54), 191, 159, and 141. The fragment ion of *m/z* 159 was attributed to the dioxygenation of the side chain. This suggests that the + 32 Da modification occurred at the side chain. M4-4 and M4-5 were identified as the dioxygenation products of PPD, both of the oxygen atoms were introduced into the side chain of the molecule.

***Metabolite M5*.** The EIC of *m/z* 509 (*m/z* 461 + 48) from the full-scan LC/MS of the HLMs incubations showed four LC peaks at 5.9, 6.8, 7.7, and 8.9 min corresponding to M5-1, M5-2, M5-3 and M5-4, respectively. The MS^2 spectra (Fig. 4I) of M5-1 and M5-3 showed fragment ions at *m/z* 491 (– 18), 473 (– 36), 455 (– 54), 437 (– 72), 191 and 143. M5-1 and M5-3 were tentatively identified as the trioxygenation products of PPD, and one of the oxygen atoms was introduced into the side chain of the molecule. The positions of other oxygenations were unclear. Due to the fragment ions of *m/z* 159 found in the MS^2 spectra (Fig. 4J) of M5-2 and M5-4, they were identified as the trioxygenation products of PPD, with two of the oxygen atoms were introduced into the side chain of the molecule. The position of the other oxygen atom was unclear.

DMD Fast Forward. Published on December 7, 2010 as DOI: 10.1124/dmd.110.036723
This article has not been copyedited and formatted. The final version may differ from this version.

Metabolites Detected in Human Hepatocytes. Fig. 5 shows the total ion and extracted ion chromatograms of the parent drug and its metabolites after 180 min of incubation with human hepatocytes. Compared with the blank sample, 19 phase I and 2 phase II metabolites were observed. Among them, metabolites M1–M4 and M5-2 were also detected in HLMs incubations as mentioned before. Four new detected metabolites may be classified into 2 types: Phase I metabolites M6 (*m*/*z* 495) from the metabolic addition of two oxygen atoms and one molecule of hydrogen (+ 34 from the parent), and Phase II metabolites M7 (*m*/*z* 653) from the addition of an oxygen atom and one molecule of glucuronic acid (+ 192 from the parent). These metabolites were numbered according to their chromatographic retention times, and the structures were elucidated through their mass spectral fragments.

Metabolites M6. Metabolites M6-1 and M6-2 gave a precursor ion at *m/z* 495, which was 34 Da larger than that of PPD, were eluted at 13.2 and 15.8 min, respectively. Their MS^2 spectra (Fig. 4K) were identical, and the major fragment ions were at *m*/*z* 477 (– 18), 459 (– 36), 441 (– 54), 423 (– 72), 191 and 159. M6-1 and M6-2 were tentatively identified as 24,25-vicinal diol derivatives of PPD, which may be generated through the ring opening reaction of the 24,25-epoxides. Since M6-1 and M6-2 are 24-epimers, the stereochemistry at C-24 is matter to discuss. It was observed that the 24*S*-epimers **2**, **4** and M7-1 were more easily be eluted from the colum than the corresponding 24*R*-epimers **3**, **5** and M7-2 under the experimental conditions. In light of this observation, bearing in mind that the epimers generated from the same parent structure usually had similar chromatographic behaviors, M6-1 and M6-2 were tentatively assigned as the 24*S*- and 24*R*-epimer, respectively.

Metabolite M7. Metabolites M7-1 and M7-2 were eluted at 16.0 and 16.9 min, respectively. Both showed a precursor ion at *m*/*z* 653, which was 192 Da larger than that of PPD. Their mass spectra were

DMD Fast Forward. Published on December 7, 2010 as DOI: 10.1124/dmd.110.036723
This article has not been copyedited and formatted. The final version may differ from this version.

identical (Fig. 4L), and the major fragment ions were at *m*/*z* 635 (– 18), 617 (– 36), 599 (– 54), 441 (– 176 – 36), 423 (– 176 – 54), 405 (– 176 – 72) and 191, indicating that two glucuronide conjugates of oxygenated PPD were produced. Furthermore, from the incubations of **2** and **3** in HLMs with the presence of UDPGA, M7-1 and M7-2 were detected after 120 min of incubation, respectively. M7-1 and M7-2 were identified as the glucuronide conjugates of **2** and **3** accordingly. Since no glucuronide conjugates of PPD were detected under the same incubation conditions, the conjugation sites of M7-1 and M7-2 were tentatively assigned to the 25-hydroxyl group, which was newly formed by biotransformation.

Structure Elucidation of Four Isolated Metabolites. In all, four most abundant metabolites (**2**–**5**) of PPD detected in the rat feces were isolated; their structures were elucidated based on extensive nuclear magnetic resonance (NMR) spectroscopic analysis. Due to their low content, other metabolites can not be readily characterized by NMR analysis. Details of the structural determination of these metabolites are hereby presented.

Compound **2** was obtained as a white amorphous powder. The molecular formula $C_{30}H_{52}O_4$ was established by high-resolution electrospray mass spectra (HR-ESI-MS) (*m*/*z* 477.3873 $[M + H]^+$) according to 5 degrees of unsaturation. Comparison of the ^1H and ^{13}C NMR (Table 1) spectral data of **2** and **1** revealed the main difference at the side chain, where the olefinic proton signal of **1** at δ 5.17 (t, J = 7.1 Hz, H-24) disappeared, suggesting that the double bond at $\Delta^{(24,25)}$ of the side chain was absent. The remaining degree of unsaturation was, therefore, attributed to a ring in the side chain. In addition, one methine signal (δ_C 87.42, d, C-24; δ_H 3.88, dd, J = 10.8, 5.6 Hz, H-24) and an OH-bearing tertiary carbon atom (δ_C 70.00, s, C-25) were observed, indicating the presence of the 20,24-epoxide moiety and a hydroxyl group at C-25. The assigned structure for **2** was confirmed by its 2D NMR spectra (Fig.

DMD Fast Forward. Published on December 7, 2010 as DOI: 10.1124/dmd.110.036723
This article has not been copyedited and formatted. The final version may differ from this version.

6) .

Compound **3** had a molecular formula of $C_{30}H_{52}O_4$, which was identical to that of **2** as indicated by HR-ESI-MS. ^{1}H-^{1}H COSY and HMBC experiments led to the same proton sequence and framework as those of **2**. Careful comparison of the ^{1}H NMR spectra (Table 1) of **3** and **2** revealed main differences at the δ values of Me-21 and Me-26, in which the former was upfield shifted (– 0.14 ppm), whereas the latter was downfield shifted (+ 0.17 ppm). Both shifts supported the inversion of the configuration at C-24. Furthermore, the α-orientation of H-24 was also supported by rotating frame nuclear Overhauser effect spectroscopy. The clear NOE cross-peak between H-24 and Me-21 suggest that both are orientated on the same face (α) of the molecule according to the drawn structure of **3** (Fig. 6).

Compound **4** had a molecular formula $C_{30}H_{50}O_4$, which was established by HR-ESI-MS (*m/z* 497.3614 $[M + Na]^+$, calc. 497.3607), with 2 mass units less than that of **2**. Comparison of the ^{13}C NMR data (Tables 1 and 2) of **2** and **4** revealed that **4** differed from **2** only at the A ring, where the hydroxyl group (δ 78.87, d) at C-3 was oxidized to a carbonyl (δ 217.83, s), which was in agreement with the two mass unit difference between them. The electron withdrawing effect of the carbonyl group caused the ^{13}C NMR resonance of C-2 and C-4 to significantly shift downfield (+ 5.50 ppm and + 7.58 ppm). The assigned structure for **4** was further confirmed by its 2D NMR spectra (Fig. 6).

Compound **5** also had a molecular formula $C_{30}H_{50}O_4$, which was established by HR-ESI-MS (*m/z* 497.3626 $[M + Na]^+$, calc. 497.3607). Analysis of the ^{1}H and ^{13}C NMR spectra of **5** revealed a close relationship with both **3** and **4**. In fact, **5** shares the same proton sequence and framework as **4**, as well as possesses the same side chain as **3**. Detailed analysis of its 2D NMR spectra allowed the unambiguous definition of the structure of **5** (Fig. 6).

Oxidation of PPD with 3-chloroperoxybenzoic acid. The EIC of *m*/*z* 477, from the full-scan LC/MS of the reaction solution of 15 min, showed three LC peaks at 18.7, 19.2, and 19.8 min (Fig. 7A); their retention times and mass spectral fragmentation patterns were identical to those of M1-1, **2**, and **3**, respectively, and the mass spectral response of **2** was stronger than those of **3**. Compounds **2** and **3** were detected in the reaction solution of 60 min, and the mass spectral response of **2** and **3** were comparable (Fig. 7B). This suggests that M1-1 might rearranged to form **3** with the prolongation of the reaction time.

Theoretically, oxidization of PPD with 3-chloroperoxybenzoic acid could resulted in the formation of 24,25-epoxides in an equivalent mixture of 24-epimers (Fig. 8). In case of the 24*R*-epimer, **2** was quickly formed through intramolecular nucleophilic attack of the oxygen atom of the hydroxyl group at C-20 to the back side of the hydrogen atom of C-24. In contrast, due to the steric hindrance posedby the β hydrogen atom at C-24 and the hydroxyl group at C-20 of the 24*S*-epimer, the speed of the intramolecular nucleophilic attack reaction to form **3** decreased. Thus, M1-1 was tentatively identified as (24*S*,25)-epoxydammarane-3,12,20-triol (**6**).

Incubations of Isolated Metabolites in HLMs. Four isolated metabolites were performed individual incubations in HLMs. Compared with the blank sample, 14, 2, 2 and 1 metabolites were detected, respectively. The metabolites from **2** may be classified into 8 types: **4** from the dehydrogenation of C-3, M3-2 from the dehydrogenation of C-3 and hydroxylation of the parent nucleus, M3-3 and M3-4 from the hydroxylation and dehydrogenation of the parent nucleus, M3-6 from the hydroxylation and dehydrogenation of the side chain, M4-1, M4-2 and M4-3 from the hydroxylation of the parent nucleus, M4-4 and M4-5 from the hydroxylation of the side chain, M5-1 and M5-3a from the dihydroxylation of the parent nucleus, M5-2 and M5-4 from the hydroxylation of both the parent

nucleus and the side chain. Two metabolites were detected from **3**: **5** from the dehydrogenation of C-3, and M5-3b from the dihydroxylation of the parent nucleus. Two hydroxylated metabolites were observed from **4**: M3-2 from the hydroxylation of the parent nucleus, and M3-5a from the hydroxylation of the side chain. The side chain hydroxylated metabolite (M3-5b) was observed from **5**.

Discussion

Ginsenosides, the major pharmacologically active components of ginseng, produce an array of pharmacological responses. Kasai et al. have assumed that the absorbed sapogenins or prosapogenins of ginseng from the digestive tract would be transformed into their 20,24-oxides, and that this biotransformative pathway is important to the pharmacological activities of ginsenosides (Kasai et al., 2000). In addition, the ginsenosides have been hypothesized to exert their pharmacological effects through their equally important metabolite, PPD (Hasegawa, 2004). However, the details regarding the metabolic pathway of PPD after absorption from the digestive tract and the structures of the metabolites were unclear. This study has determined its metabolically labile sites and its metabolite profile in humans.

Since the animal experimentes shows that the peak concentration of PPD in rat liver was about 20 μM after an oral administration of 50 mg/kg. And in our preliminary experimentes, we found that the types of PPD metabolites detected in human liver microsomes changed unconspicuous in the concentration range of 10-50 μM. Because higher concentration of the metabolites make for the mass-spectrometric detection, we choose 50 μM as the final incubation concentration. Furthermore, similar PPD metabolites were found in both human liver microsomes and rat feces receiving PPD administration. Our previous ^{3}H radiolabelled experiment on this compound shows that about 74.2% of the orally administered dose is excreted in the feces within 48 h. In order to obtain the reference substances of PPD metabolites, 20 rats were given continuous oral PPD administration for 11 days, and the rat feces samples were collected within a period of 0–288 h (48 h after the last dosing) for chemical examination.

Using liquid chromatography-electrospray ionization (ESI) ion trap mass spectrometry, 24

metabolites were found in HLMs and human hepatocytes. The chemical structures of the metabolites were elucidated by their accurate mass, mass spectral fragmentation patterns, and comparison with isolated standards. Our experiments suggest that the 24,25-double bond of PPD is highly susceptible to oxidative biotransformation. It was first oxidized by liver monooxygenase to form the 24,25-epoxide metabolites. Due to the intramolecular nucleophilic attack of the 20-hydroxyl group, the 24,25-epoxide metabolites rearranged to the 20,24-oxide form (**2** and **3**), followed by further hydroxylation, dehydrogenation and glucuronide conjugation to form M2–M5 and M7. The corresponding 24,25-vicinal diol metabolites (M6) were also formed through the possible ring opening reaction. It was found that the mass spectral response of **2** and **3** were comparable at the same concentration under our experimental conditions. Furthermore, in the EIC of *m*/*z* 477, from the full-scan LC/MS of the HLMs and human hepatocytes incubations of PPD, the mass spectral response of **2** was stronger than those of **3**. These results indicate that the formation of 20,24-oxides of PPD in humans was stereoselective, in particular, the content of 24*S*-epimer was higher than that of 24*R*-epimer.

For PPD undergoing extensive sequential metabolism in HLMs and human hepatocytes, it is very difficult to identify definitive metabolic pathways. By performing individual incubations of isolated metabolites, possible metabolic pathways of PPD in HLMs were proposed. Among these isolated metabolites, **2** underwent extensive biotransformation with a metabolite profile similar to that of PPD for most of the applicable metabolites. This suggests that **2** represents an important oxygenated metabolite responsible for further hydroxylation and dehydrogenation in humans. In contrast, metabolite **3** only underwent dehydrogenation and dihydroxylation to form metabolites **5** and M5-3b. Furthermore, metabolite **4** underwent hydroxylation to form 2 hydroxylated metabolites, whereas,

DMD Fast Forward. Published on December 7, 2010 as DOI: 10.1124/dmd.110.036723
This article has not been copyedited and formatted. The final version may differ from this version.

metabolite **5** only underwent hydroxylation to form a small quantity of M3-5b. These results indicate that the enzyme-mediated biotransformation of PPD metabolites having a substituted tetrahydrofuran ring, such as **2**, **3**, **4** and **5**, might also be stereoselective. It seems that the 24*S*-epimers were more susceptible to further oxidative biotransformation than 24*R*-epimers in HLMs. From the results of this study, the metabolic pathways of PPD in humans have been postulated (Fig. 9).

It is believed that, epoxides formed by bioactivation readily confer covalent binding to thiol group containing proteins by nucleophilic attack. The covalent binding and formation of drug-protein adducts are generally considered to be related to drug toxicity (Zhou et al., 2005). To evaluate their reactivity, nucleophilic GSH (5 mM) was incorporated as an exogenous agent to trap 24,25-epoxide metabolites of PPD in incubations of NADPH-supplemented human liver microsomes. However, LC/MS analyses of the incubation mixture after 60 min indicated that there were no GSH conjugates observed. Neither GSH conjugates were detected in human hepatocyte incubations responsible for the 24,25-epoxide metabolites. It appears that the transformation of 24,25-epoxide metabolites of PPD to corresponding GSH conjugates may be very limited in humans.

Complete and reliable assignment of spectroscopic data is crucial for confirming chemical structures and evaluating purity of compounds. To the best of our knowledge, the ^{13}C NMR data of natural products **2** (Appendino et al., 1992), **3** (Yosioka et al., 1972), **4** (Appendino et al., 1992), and **5** (Appendino et al., 1992; Valverde et al., 1985) have been completely assigned in previous works. However, only their incomplete ^{1}H NMR assignments have been reported. In this study, a thorough spectroscopic analysis of compounds **2**–**5** has been undertaken. Herein, a complete assignment of the ^{1}H NMR data of compounds **2**–**5** is presented based on an extensive analysis of DEPT and 2D NMR spectra, including HSQC, ^{1}H-^{1}H COSY, HMBC, and NOESY (Tables 1 and 2).

In conclusion, this *in vitro* study reveals that PPD is extensively metabolized in human liver microsomes and human hepatocytes. Carbon-carbon double bond epoxidation were the primary metabolic reaction observed, to yield the 24,25-epoxide metabolites followed by hydrolysis and rearrangement to form the corresponding 24,25-vicinal diol derivatives (M6) and the 20,24-oxide form (**2** and **3**). Further sequential metabolites (M2–M5) were also detected through the hydroxylation and/or dehydrogenation of **2** and **3**. One thing worth mentioning is that all of the Phase I metabolites except for M1-1 possess a hydroxyl group at C-25 of the side chain, which was newly formed by biotransformation. Furthermore, two glucuronide conjugates attribute to **2** and **3** were detected in human hepatocyte incubations after 180 min of incubation, and the conjugation sites of them were tentatively assigned to the 25-hydroxyl group. These findings along with the fact that no glucuronide conjugates of PPD were detected under the same incubation conditions strongly suggested that the formation of the 25-hydroxyl group is very important for the elimination of PPD. Results from this work are important for understanding the metabolism of PPD and related ginsenosides in humans and provide useful information that may act as a reference for the clinical pharmacology.

Acknowledgments.

We would like to thank Ms. Jia Liu, and Mr. Xin Zhou for their help with the experiment periods.

Authorship contributions

Participated in research design: Zhong, Chen, L. Li and D. Li.

Conducted experiments: L. Li and D. Li.

Contributed new reagents or analytic tools: Zhong, Chen and L. Li.

Performed data analysis: Zhong, Chen and L. Li.

Contributed to the writing of the manuscript: Zhong, Chen and L. Li.

Other: Zhong and Chen acquired funding for the research.

References

Appendino G, Garibold P, Wollenweber E, Sironi A and Molineri H (1992) Triterpenes from the frond exudate of the fern *Notholaena greggii*. *Phytochemistry* **31:**923–927.

Chang SJ, Suh JS, Jeon BH, Nam KY and Park HK (1994) Vasorelaxing effect by protopanaxatriol and protopanaxadiol of *Panax ginseng* in the pig coronary artery. *Koryo Insam Hakhoechi* **18:**95–101.

Hasegawa H (2004) Proof of the mysterious efficacy of ginseng: basic and clinical trials: metabolic activation of ginsenoside: deglycosylation by intestinal bacteria and esterification with fatty acid. *J Pharmacol Sci* **95**:153–157.

Hui YZ, Yang ZR, Yang ZQ and Ge Q (2006) Antidepressant compositions containing 20(*S*)-protopanaxadiol extracted from ginsenoside. *China Patent* CN 200610027507.1.

Kasai R, Hara K, Dokan R, Suzuki N, Mizutare T, Yoshihara S and Yamasaki K (2000) Major metabolites of ginseng sapogenins formed by rat liver microsomes. *Chem Pharm Bull* **48:**1226–1227.

Kim DH, Jung JS, Moon YS, Sung JH, Suh HW, Kim YH and Song DK (2003) Inhibition of intracerebroventricular injection stress-inductd plasma corticosterone levels by intracerebroventricularly administered compound K, a ginseng saponin metabolite, in mice. *Biol Pharm Bull* **26:**1035–1038.

Lee JY, Shin JW, Chun KS, Park KK, Chung WY, Bang YJ, Sung JH and Surh YJ (2005a) Antitumor promotional effects of a novel intestinal bacterial metabolite (IH-901) derived from the protopanaxadiol-type ginsenosides in mouse skin. *Carcinogenesis* **26:**359–367.

Lee SH, Seo GS, Ko G, Kim JB and Sohn DH (2005b) Anti-inflammatory activity of

20(*S*)-protopanaxadiol: enhanced heme oxygenase I expression in RAW 264.7 cells. *Planta Med* **71:**1167–1170.

Lee WM, Kim SD, Kim KS, Song YB, Kwak YS, Cho JY, Park HJ, Oh JW and Rhee MH (2006) Protopanaxadiol modulates LPS-induced inflammatory activity in murine macrophage RAW264.7 cells. *J Ginseng Res* **30:**181–187.

Leung KW, Leung FP, Mak NK, Tombran-Tink J, Huang Y and Wong Ricky NS (2009) Protopanaxadiol and protopanaxatriol bind to glucocorticoid and oestrogen receptors in endothelial cells. *Br J Pharmacol* **156:**626–637.

Li G, Wang ZH, Sun YX, Liu K and Wang ZR (2006) Ginsenoside 20(*S*)-protopanaxadiol inhibits the proliferation and invasion of human fibrosarcoma HT1080 cells. *Basic Clin Pharmacol Toxicol* **98:**588–592.

Liu GY, Bu XX, Yang H and Jia WWG (2007) 20*S*-Protopanaxadiol-induced programmed cell death in glioma cells through caspase-dependent and -independent pathways. *J Nat Prod* **70:**259–264.

Liu Y, Li W, Li P, Deng MC, Yang SL and Yang L (2004) The inhibitory effect of intestinal bacterial metabolite of ginsenosides on CYP3A activity. *Biol Pharm Bull* **27:**1555–1560.

Liu Y, Zhang JW, Li W, Ma H, Sun J, Deng MC and Yang L (2006) Ginsenoside metabolites, rather than naturally occurring ginsenosides, lead to inhibition of human cytochrome P450 enzymes. *Toxicol Sci* **91:**356–364.

Park EK, Choo MK, Oh JK, Ryu JH and Kim DH (2004) Ginsenoside Rh2 reduces ischemic brain injury in rats. *Biol Pharm Bull* **27:**433–436.

Popovich DG and Kitts DD (2004) Ginsenosides 20(*S*)-protopanaxadiol and Rh2 reduce cell proliferation and increase sub-G1 cells in two cultured intestinal cell lines, Int-407 and Caco-2.

Can J Physiol Pharmacol **82:** 183–190.

Shibata S, Tanaka O, Ando T, Sado M, Tsushima S and Ohsawa T (1966) Chemical studies on oriental plant drugs. XIV. Protopanaxadiol, a genuine sapogenin of ginseng saponins. *Chem Pharm Bull* **14:**595–600.

Shin YH, Kim SC, Han JW, Kim DH, Han SS, Shin DH and Nah SY (1997) Study on ginseng protopanaxadiol and protopanaxatriol saponins-induced antinociception. *Korean J Physiol Pharmacol* **1:**143–149.

Tanaka O, Nagai M and Shibata S (1966) Chemical studies on the oriental plant drugs. A genuine sapogenin of ginseng. *Chem Pharm Bull* **14:**1150–1156.

Usami Y, Liu YN, Lin AS, Shibano M, Akiyama T, Itokawa H, Morris-Natschke SL, Bastow K, Kasai R and Lee KH (2008) Antitumor agents. 261. 20(*S*)-Protopanaxadiol and 20(*S*)-protopanaxatriol as antiangiogenic agents and total assignment of ^{1}H NMR spectra. *J Nat Prod* **71:**478–481.

Valverde S, Escudero J, Lopez JC and Rabanal RM (1985) Two terpenoids from *Salvia bicolor*. *Phytochemistry* **24:**111–113.

Yosioka I, Yamauchi H and Kitagawa I (1972) Lichen triterpenoids. V. on the neutral triterpenoids of *Pyxine endochrysina* nyl. *Chem Pharm Bull* **20:**502–513.

Yu Y, Zhou Q, Hang Y, Bu XX and Jia W (2007) Antiestrogenic effect of 20*S*-protopanaxadiol and its synergy with tamoxifen on breast cancer cells. *Cancer* **109:**2374–2382.

Zhang R, Xu HL, Yu XF, Qu SC, Chen MX and Sui DY (2008) Effect of 20(*S*)-protopanaxadiol on SMMC-7721 human liver cancer in vivo and in vitro. *Chin Pharmacol Bull* **24:**1504–1508.

Zhou SF, Chan E, Duan W, Huang M and Chen YZ (2005) Drug bioactivation, covalent binding to target proteins and toxicity relevance. *Drug Metab Rev* **37**: 41–213.

Footnote

This work was supported by the National Science and Technology Major Project “Key New Drug Creation and Manufacturing Program”, China [Grant 2009ZX09301-001].

Legends for figures

Fig. 1. Chemical structure of 20(*S*)-protopanaxadiol (**1**, PPD).

Fig. 2. Full scan mass spectrum (A) and MS^2 spectrum of 20(*S*)-protopanaxadiol (B). The MS^2 data were obtained from the *m/z* 425.3 ion as the precursor for collision-induced dissociation.

Fig. 3. Extracted ion $[M + H]^+$ chromatograms of 20(*S*)-protopanaxadiol metabolites in HLMs incubations. (A) with NADPH; (B) without NADPH. Twenty detected metabolites are labeled as M1 (*m*/*z* 477), M2 (*m*/*z* 475), M3 (*m*/*z* 491), M4 (*m*/*z* 493), and M5 (*m*/*z* 509), and the parent compound is labeled as PPD. These metabolites were numbered according to their chromatographic retention times.

Fig. 4. MS^2 spectra of 20(*S*)-protopanaxadiol metabolites on ion trap MS; A : M1 (*m*/*z* 477.4); B: M2 (*m*/*z* 475.4); C: M3-1, M3-3 and M3-4 (*m*/*z* 491.4); D: M3-2 (*m*/*z* 491.4); E: M3-5 (*m*/*z* 491.4); F: M3-6 (*m*/*z* 491.4); G: M4-1–M4-3 (*m*/*z* 493.4); H: M4-4 and M4-5 (*m*/*z* 493.4); I: M5-1 and M5-3 (*m*/*z* 509.4); J: M5-2 and M5-4 (*m*/*z* 509.4); K: M6 (*m*/*z* 495.4); L: M7 (*m*/*z* 653.4). All of the MS^2 data were obtained from the respective $[M + H]^+$ ions as the precursors for collision-induced dissociation.

Fig. 5. Extracted ion $[M + H]^+$ chromatograms of 20(*S*)-protopanaxadiol metabolites in human hepatocytes incubations. (A) incubated with 20(*S*)-protopanaxadiol for 3 h; (B) incubated without 20(*S*)-protopanaxadiol for 3 h. Twenty-one detected metabolites are labeled as M1 (*m*/*z* 477), M2 (*m*/*z* 475), M3 (*m*/*z* 491), M4 (*m*/*z* 493), M5 (*m*/*z* 509), M6 (*m*/*z* 495), and M7 (*m*/*z* 653), and the parent

compound is labeled as PPD. These metabolites were numbered according to their chromatographic retention times.

Fig. 6. Selected HMBC and NOESY correlations for the substituted tetrahydrofuran side chain of the metabolites **2**, **3**, **4** and **5.** The HMBC correlations were used for the identification of their framework and the NOESY correlations were used for the determination of the stereochemistry of C-24.

Fig. 7. Extracted ion $[M + H]^+$ chromatograms of the reaction mixture of 20(*S*)-protopanaxadiol (100 μM) and 3-chloroperoxybenzoic acid (10 μM). (A) after stirred at room temperature for 15 min; (B) after stirred at room temperature for 60 min. The products are labeled as M1 (*m*/*z* 477.4) and the reactant is labeled as PPD.

Fig. 8. Plausible formation pathways of M1-1, M1-2 and M1-3 from 20(*S*)-protopanaxadiol by chemical oxidation with 3-chloroperoxybenzoic acid.

Fig. 9. Proposed *in vitro* metabolic pathways of 20(*S*)-protopanaxadiol in humans (Structure in bracket is proposed intermediate that was not detected). Structures in the dashed line rectangle were metabolites from the same precursor. Character “Glu” of M7-1 and M7-2 refers to the glucuronic acid residue.

DMD Fast Forward. Published on December 7, 2010 as DOI: 10.1124/dmd.110.036723
This article has not been copyedited and formatted. The final version may differ from this version.

Tables

Table 1. NMR Data of M1-2 (**2**) and M1-3 (**3**) in $CDCl_3$

	2				**3**		
	δH (*J* in Hz)	δC	HMBC	NOESY	δH (*J* in Hz)	δC	NOESY
1	1.72[a]	38.93, t	2, 5		1.72[a]	38.90, t	
	0.98[a]		2		0.98[a]		
2	1.85[a]	28.56, t	1		1.88[a]	28.58, t	
3	3.20, dd (11.3, 5.0)	78.87, d	1, 4, 28, 29	5, 9, 28	3.18, dd (11.4, 5.0)	78.85, d	5, 28
4		39.75, s				39.70, s	
5	0.75, dd (11.3, 1.4)	55.95, d	3, 4, 10, 28, 29	3, 9, 28	0.72, dd (10.9, 1.7)	55.94, d	3, 9, 28
6	1.56[a]	18.32, t	10		1.58[a]	18.26, t	
	1.49[a]		5		1.46[a]		
7	1.45[a]	34.78, t	6		1.45[a]	34.79, t	
	1.30[a]		5, 9, 10		1.31[a]		
8		39.75, s				39.70, s	
9	1.48[a]	50.25, d	8, 11	5, 12, 30	1.46[a]	50.47, d	5, 12, 30
10		37.18, s				37.12, s	
11	1.93[a]	32.23, t	8		1.90[a]	31.29, t	
	1.75[a]				1.64[a]		
12	3.53, ddd (10.8, 10.6, 4.8)	70.57, d	9	9, 17, 30	3.50, ddd (10.5, 10.4, 4.6)	70.99, d	9, 17, 30
13	1.70[a]	48.81, d	11, 17, 30	18	1.69[a]	49.37, d	18
14		52.17, s				52.00, s	
15	1.50[a]	31.67, t	13, 14, 16		1.56[a]	32.62, t	
	1.11[a]		14, 17		1.13[a]		
16	1.85[a]	25.07, t	13, 14		1.87[a]	25.00, t	
	1.32[a]		13, 17		1.33[a]		
17	2.23, ddd (9.8, 9.7, 4.4)	48.92, d	15, 20	12, 21, 30	2.18, ddd (10.0, 9.6, 3.6)	47.94, d	12
18	0.91, s	17.79, q	7, 8, 9, 11, 14	13, 19	0.98, s	18.18, q	13, 19
19	1.01, s	15.47, q	1, 5, 9, 10	18, 29	0.96, s	15.35, q	18, 29
20		87.15, s				86.49, s	
21	1.23, s	27.45, q	17, 20, 22	17, 26	1.09, s	27.63, q	24
22	1.98[a]	31.64, t			1.93[a]	31.19, t	
	1.60[a]				1.66[a]		
23	1.73[a]	27.45, t	25		1.64[a]	27.41, t	
	1.55[a]		25		1.28[a]		
24	3.88, dd (10.8, 5.6)	87.42, d	25	27	3.84, dd (8.8, 6.6)	85.40, d	21, 27
25		70.00, s				70.08, s	
26	1.10, s	24.21, q	24, 25, 27	21	1.27, s	26.11, q	
27	1.27, s	28.01, q	24, 25, 26	24	1.26, s	27.91, q	24
28	0.97, s	28.88, q	3, 4, 5, 29	3, 5	0.85, s	27.97, q	3, 5
29	0.78, s	15.31, q	3, 4, 5, 28	19	0.77, s	15.26, q	19
30	0.88, s	16.29, q	8, 13, 14, 15	9, 12, 17	0.89, s	16.32, q	9, 12

[a] Overlapping signals. [b] s = singlet, d = doublet, t = triplet, q = quartet.

DMD Fast Forward. Published on December 7, 2010 as DOI: 10.1124/dmd.110.036723
This article has not been copyedited and formatted. The final version may differ from this version.

Table 2. NMR Data of M2-1 (**4**) and M2-2 (**5**) in $CDCl_3$

	4				**5**		
	δH (*J* in Hz)	δC	HMBC	NOESY	δH (*J* in Hz)	δC	NOESY
1	1.95 [a]	39.71, t	3, 5	12	1.96 [a]	39.74, t	2, 2' 12
	1.49 [a]		3	2, 2'	1.47 [a]		12
2	2.49, ddd (15.8, 9.5, 7.9)	34.06, t	1, 3, 10	1', 19	2.52, ddd (16.2, 9.6, 7.6)	34.06, t	1, 19, 29
	2.44, ddd (15.8, 7.7, 4.4)		1, 3, 10	1', 5, 28	2.43, ddd (15.8, 7.8, 4.3)		1, 5, 28
3		217.83, s				217.84, s	
4		47.33, s				47.35, s	
5	1.40 [a]	55.24, d	3, 19, 28, 29	2', 9, 28, 30	1.39 [a]	55.32, d	2', 9, 28
6	1.52 [a]	19.67, t	5		1.50 [a]	19.61, t	
7	1.52 [a]	34.00, t	5		1.50 [a]	34.06, t	
	1.34 [a]		5, 9		1.30 [a]		
8		39.59, s				39.58, s	
9	1.57 [a]	49.52, d	1, 5, 18	5, 12, 30	1.56 [a]	49.79, d	5, 12, 30
10		36.82, s				36.81, s	
11	1.93 [a]	32.03, t	8, 10		1.90 [a]	31.18, t	
	1.56 [a]		10		1.65 [a]		
12	3.53, ddd (10.4, 10.3, 4.6)	70.35, d		1, 9, 17, 30	3.50, ddd (10.6, 10.6, 4.6)	70.79, d	1, 9, 17, 30
13	1.73 [a]	48.84, d	12, 30	18, 21	1.70 [a]	49.48, d	18
14		52.15, s				51.98, s	
15	1.55 [a]	31.60, t	17		1.56 [a]	31.64, t	
	1.10 [a]		14, 17, 30		1.17 [a]		
16	1.86 [a]	25.01, t	14		1.89 [a]	24.97, t	
	1.32 [a]		13, 17		1.34 [a]		
17	2.27, ddd (10.8, 10.8, 4.5)	48.90, d	20, 21	12, 21, 30	2.22, ddd (11.0, 11.0, 3.5)	47.88, d	12, 30
18	0.93, s	17.67, q	7, 8, 9, 14	13, 19	1.01, s	16.07, q	13, 19
19	1.05, s	15.12, q	1, 5, 9, 10	18, 29	1.07, s	15.04, q	18, 29
20		87.11, s				86.47, s	
21	1.24, s	28.05, q	17, 20, 22	17, 26	1.09, s	26.11, q	24
22	1.96 [a]	32.17, t	21		1.90 [a]	32.57, t	24
	1.55 [a]		21		1.65 [a]		
23	1.70 [a]	28.51, t			1.68 [a]	28.55, t	
	1.30 [a]				1.35 [a]		
24	3.88, dd (10.8, 5.4)	87.40, d	25	26, 27	3.85, dd (9.0, 6.6)	85.41, d	21, 22, 26
25		70.01, s				70.08, s	
26	1.11, s	24.19, q	24, 25, 27	21	1.28, s	27.90, q	21, 24
27	1.28, s	28.86, q	24, 25, 26	24	1.27, s	27.59, q	
28	1.08, s	26.71, q	3, 4, 5, 29	2', 5	0.95, s	26.60, q	2', 5
29	1.05, s	20.92, q	3, 4, 5, 28	19	1.03, s	20.92, q	2, 19
30	0.98, s	16.09, q	8, 13, 14, 15	5, 9, 12, 17	0.90, s	18.06, q	5, 9, 12, 17

[a] Overlapping signals. [b] s = singlet, d = doublet, t = triplet, q = quartet.

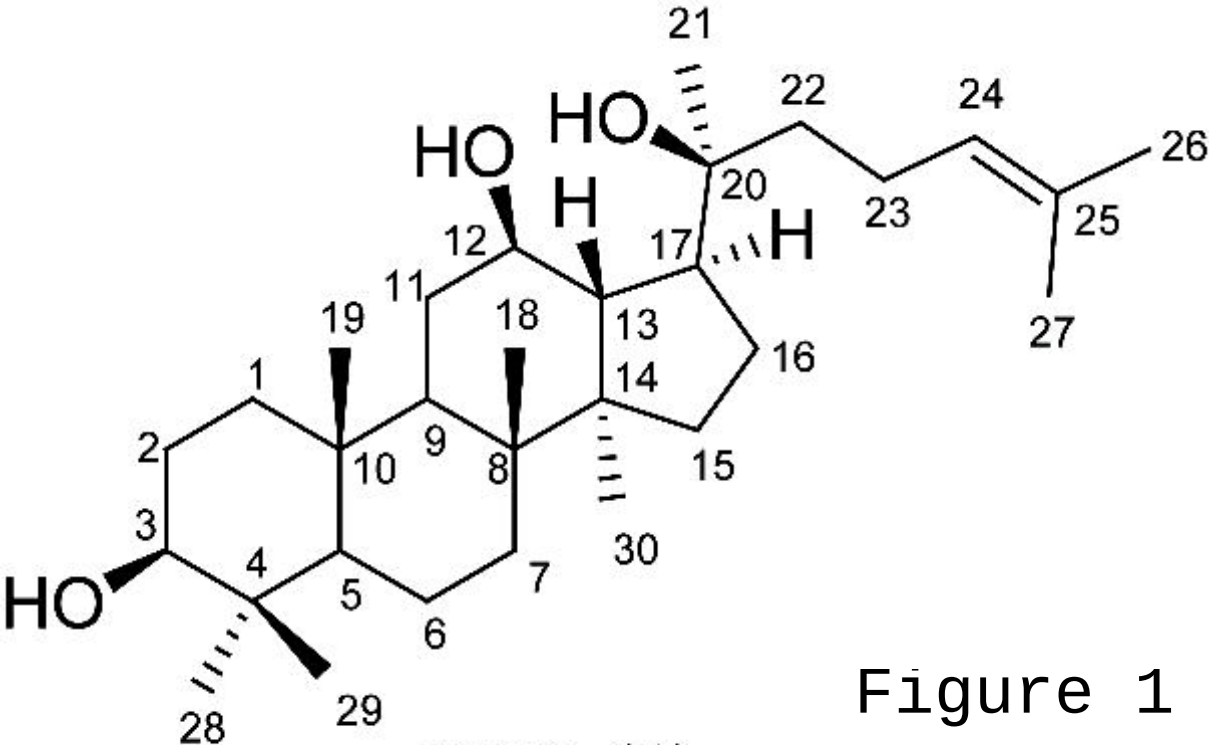

PPD (1)

Figure 1

Figure 2

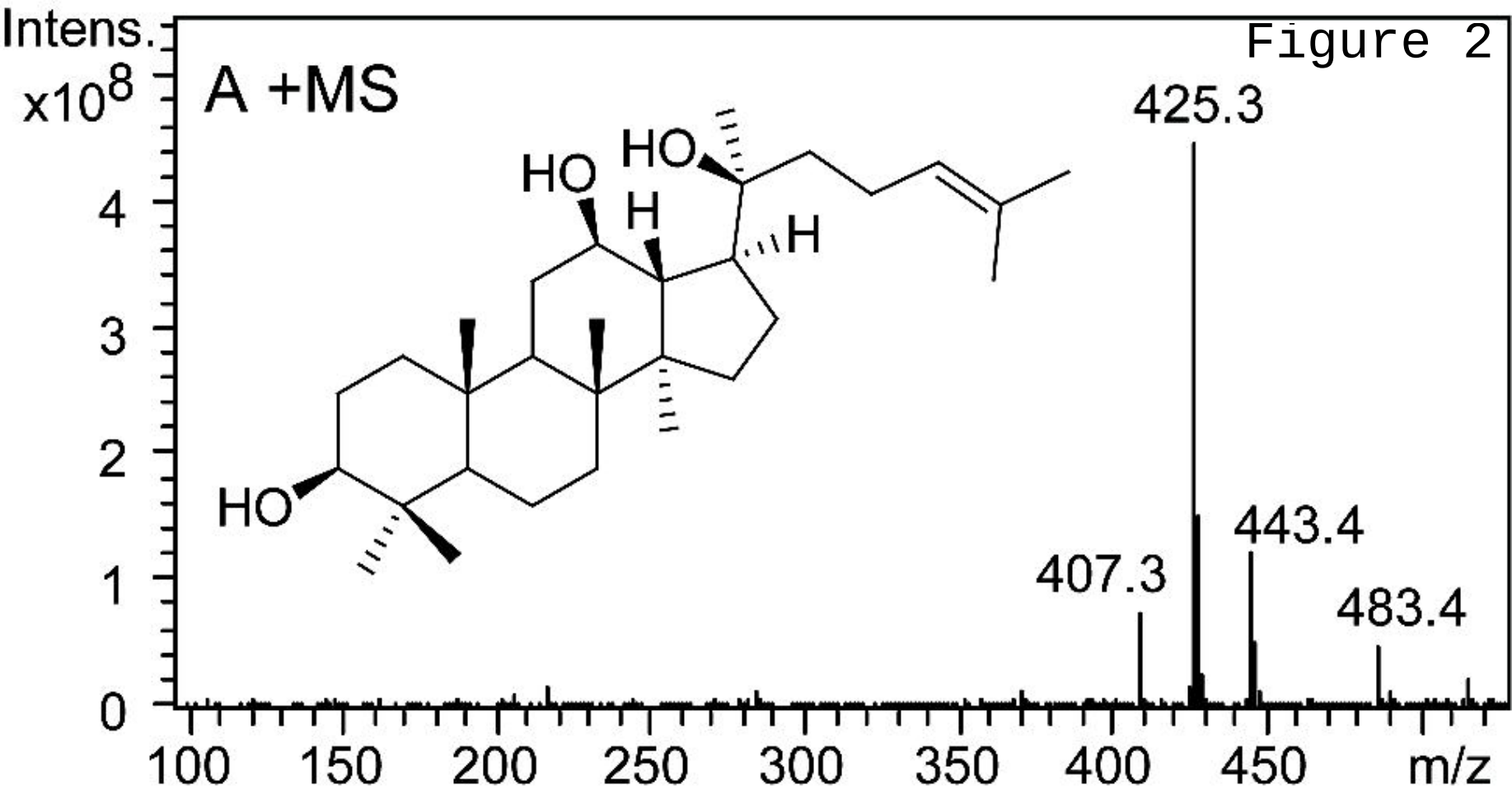
Intens.
x10^8
A +MS
425.3
443.4
407.3
483.4
HO
HO
HO
H
H
0
1
2
3
4
100
150
200
250
300
350
400
450
m/z

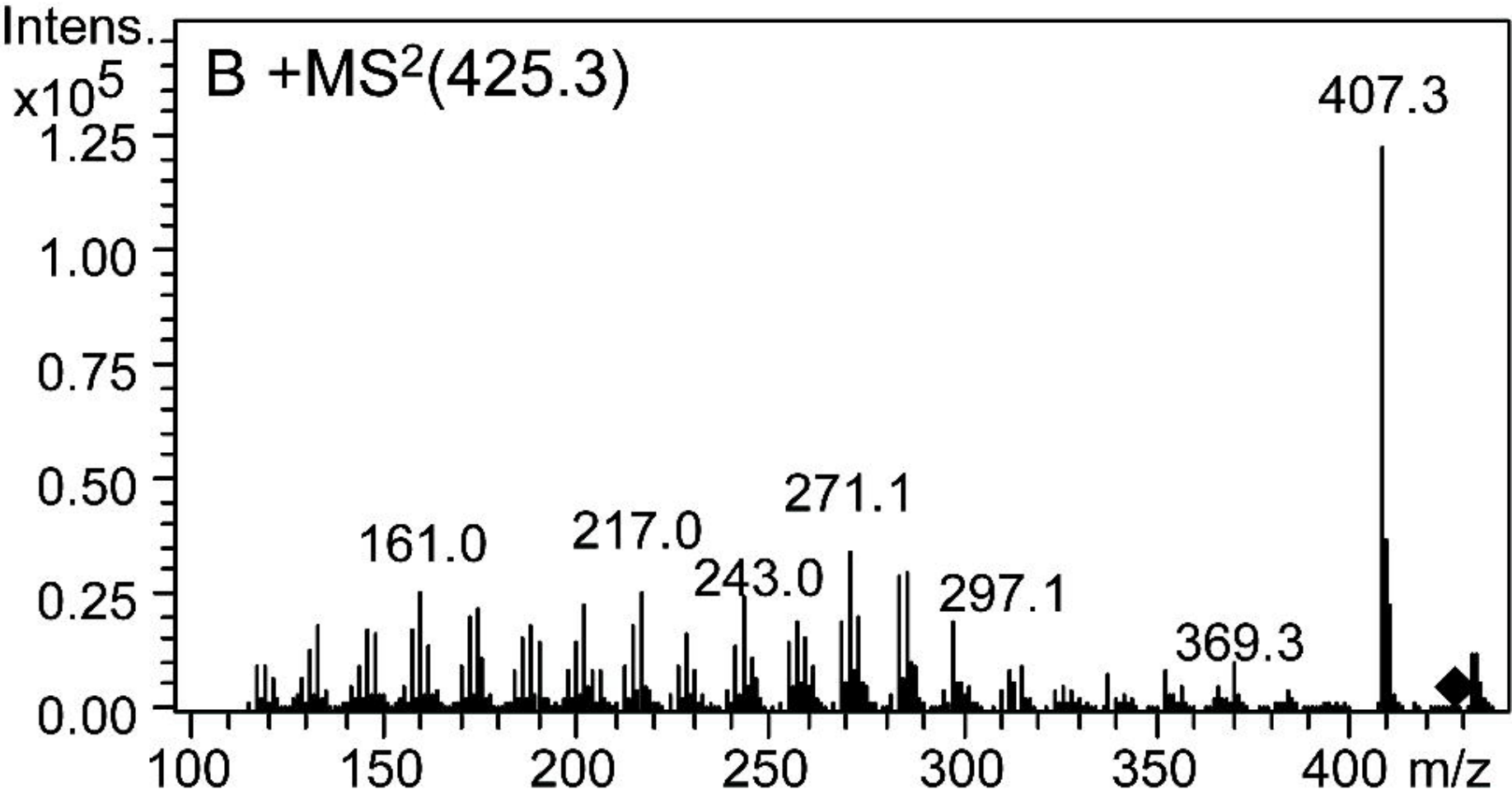
Intens.
x10^5
B +MS^2(425.3)
407.3
271.1
217.0
161.0
243.0
297.1
369.3
1.25
1.00
0.75
0.50
0.25
0.00
100
150
200
250
300
350
400
m/z

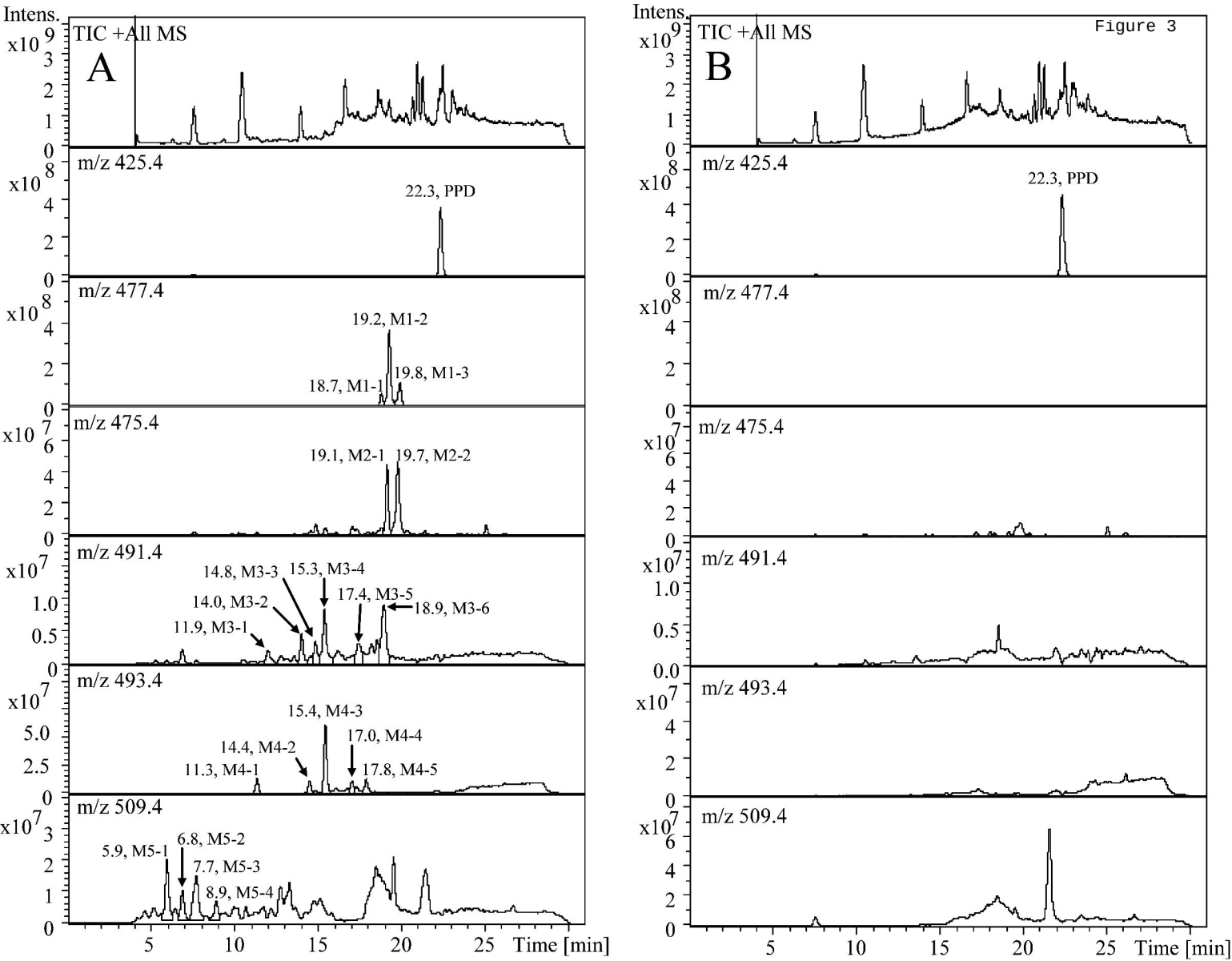
Intens.
TIC +All MS
A
m/z 425.4
22.3, PPD
m/z 477.4
19.2, M1-2
19.8, M1-3
18.7, M1-1
m/z 475.4
19.1, M2-1
19.7, M2-2
m/z 491.4
14.8, M3-3
15.3, M3-4
14.0, M3-2
17.4, M3-5
18.9, M3-6
11.9, M3-1
m/z 493.4
15.4, M4-3
17.0, M4-4
14.4, M4-2
11.3, M4-1
17.8, M4-5
m/z 509.4
5.9, M5-1
6.8, M5-2
7.7, M5-3
8.9, M5-4
Time [min]
Intens.
TIC +All MS
Figure 3
B
m/z 425.4
22.3, PPD
m/z 477.4
m/z 475.4
m/z 491.4
m/z 493.4
m/z 509.4
Time [min]

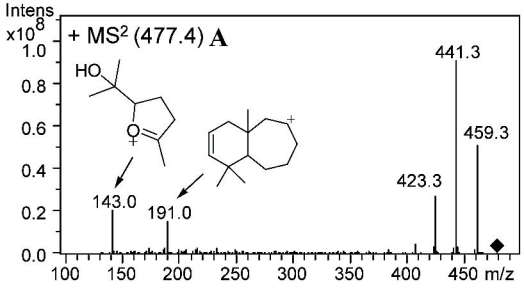

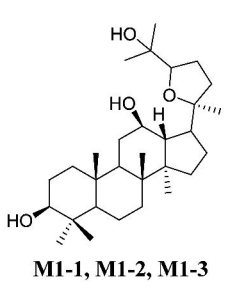

M1-1, M1-2, M1-3

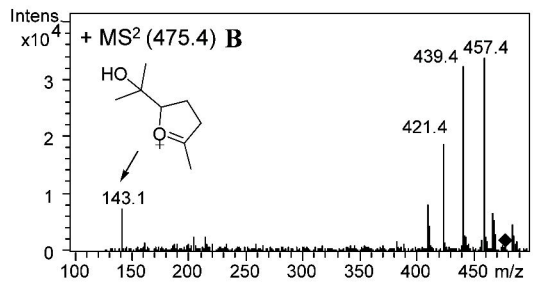

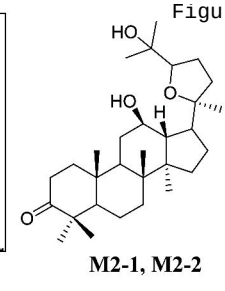

M2-1, M2-2

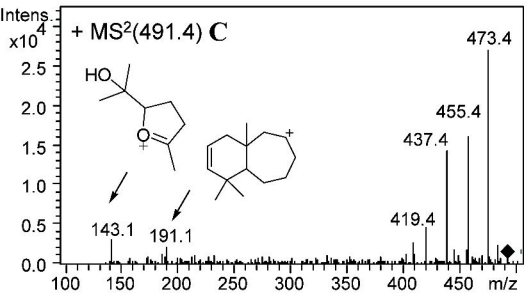

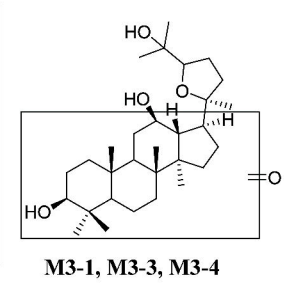

M3-1, M3-3, M3-4

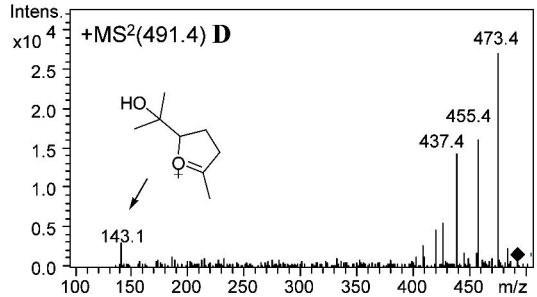

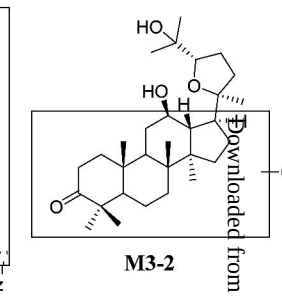

M3-2

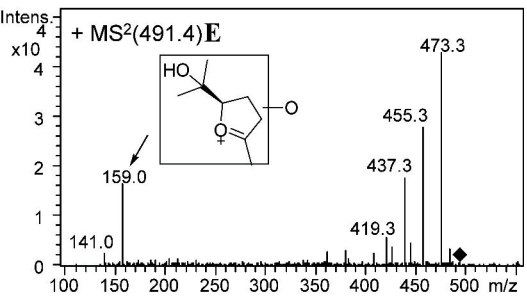

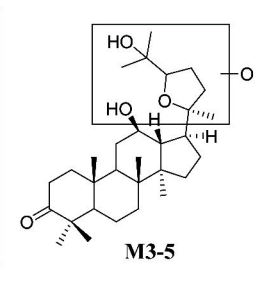

M3-5

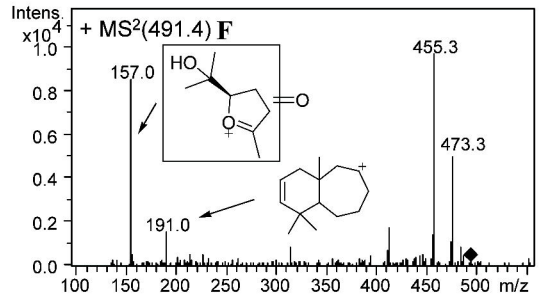

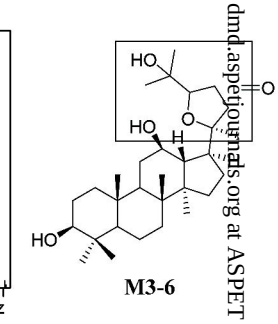

M3-6

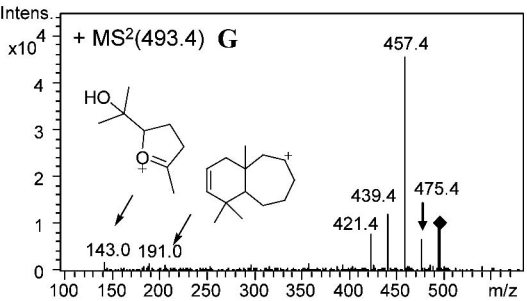

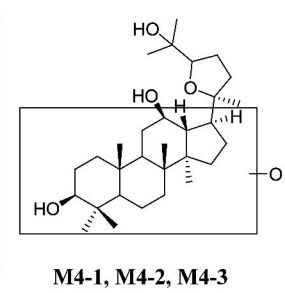

M4-1, M4-2, M4-3

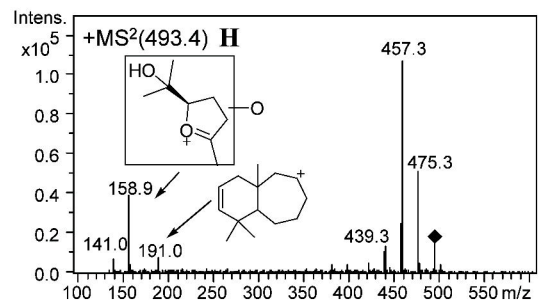

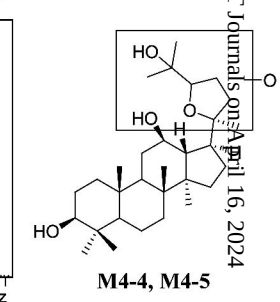

M4-4, M4-5

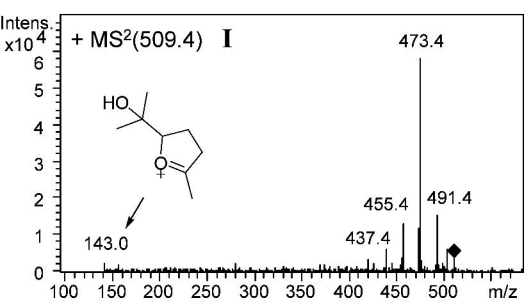

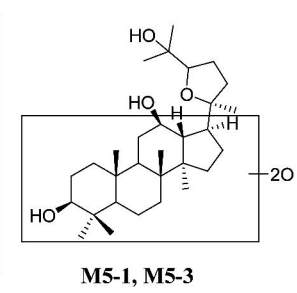

M5-1, M5-3

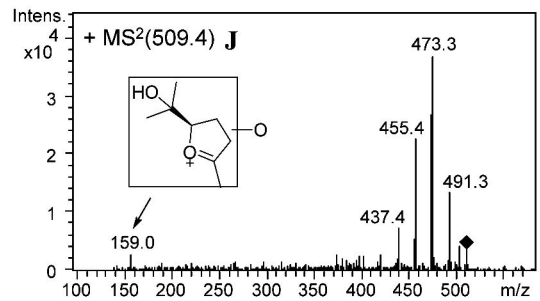

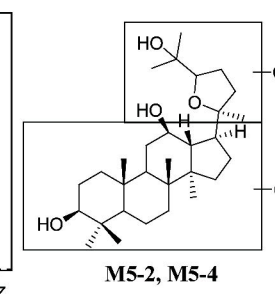

M5-2, M5-4

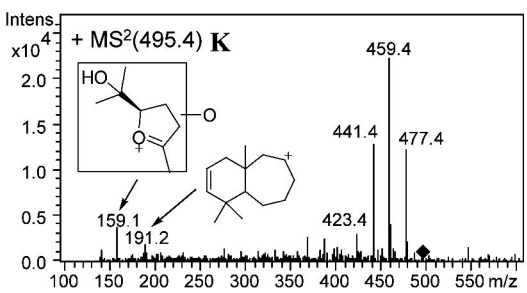

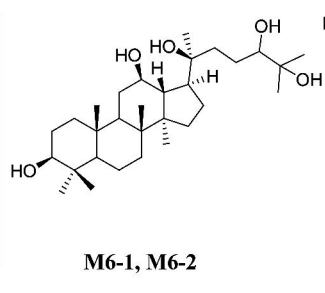

M6-1, M6-2

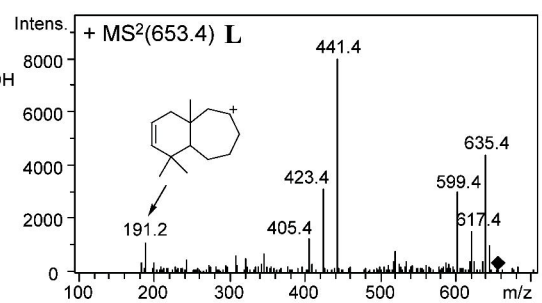

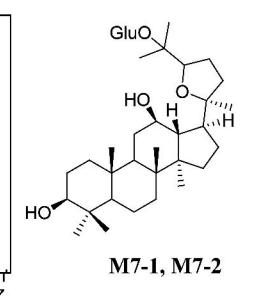

M7-1, M7-2

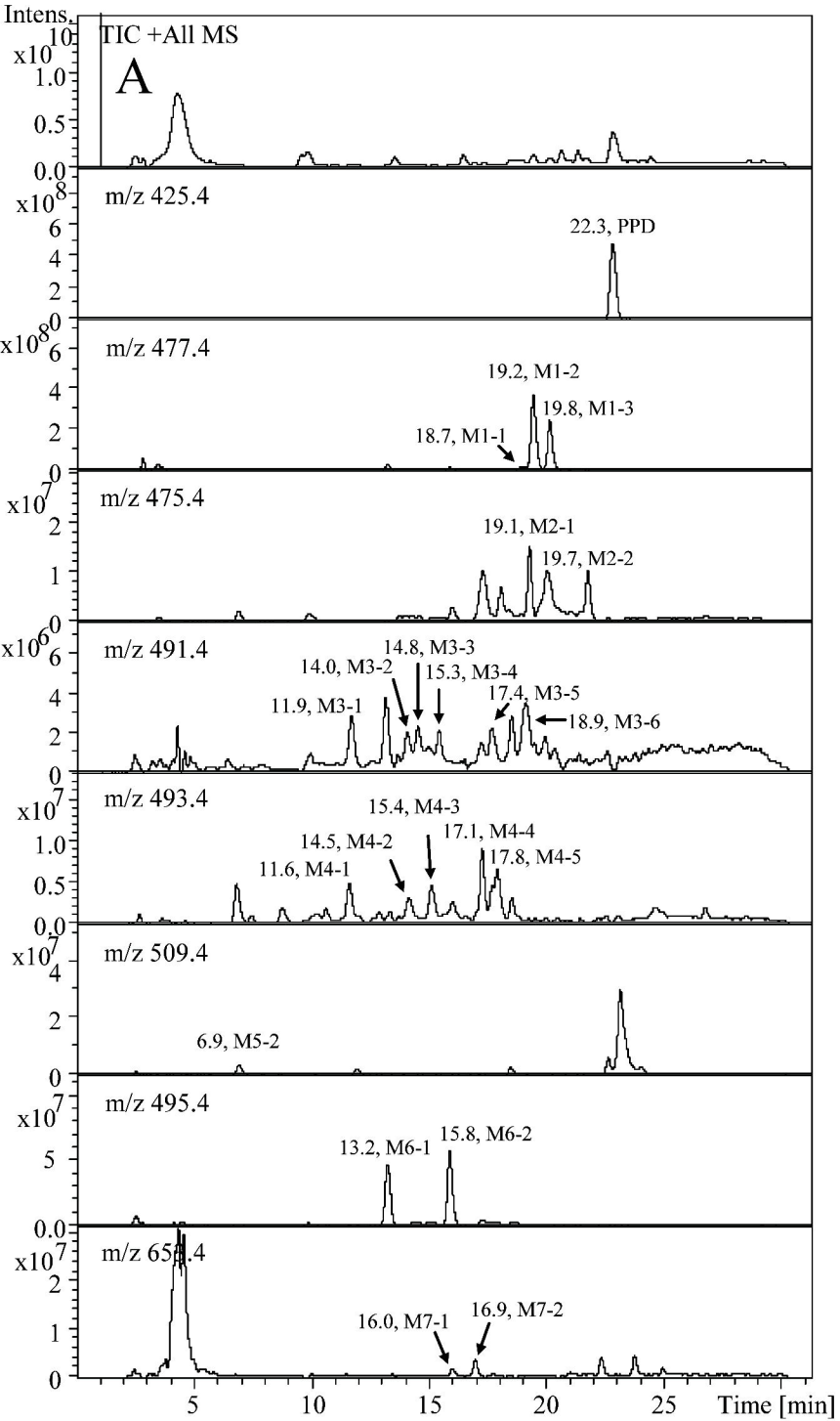

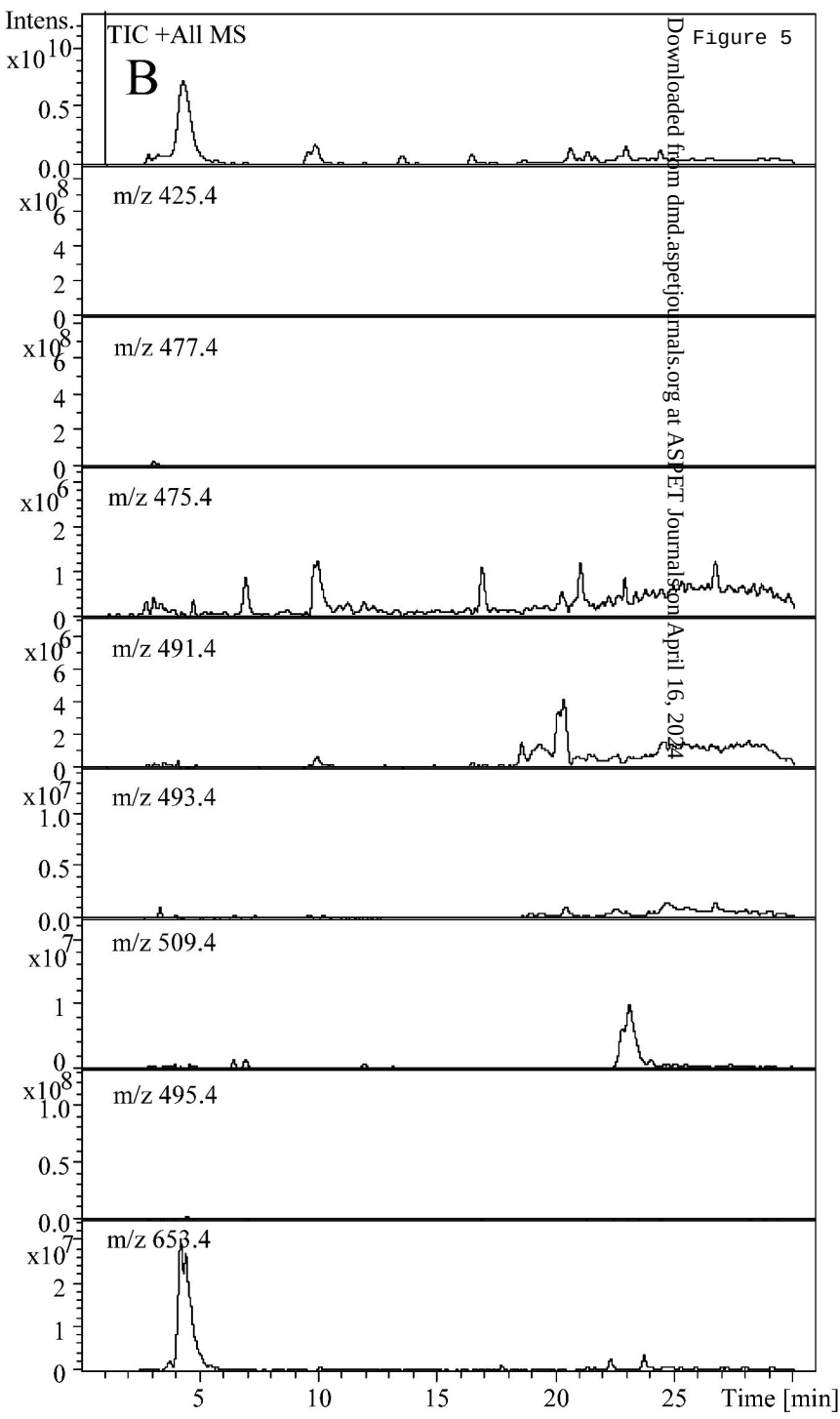

Figure 6

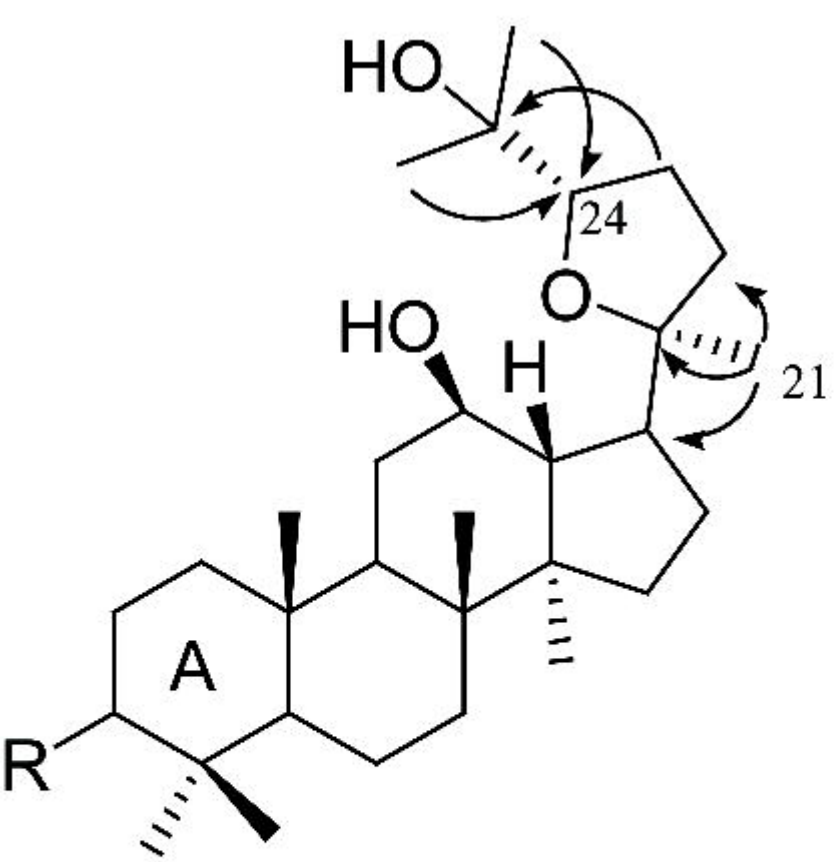

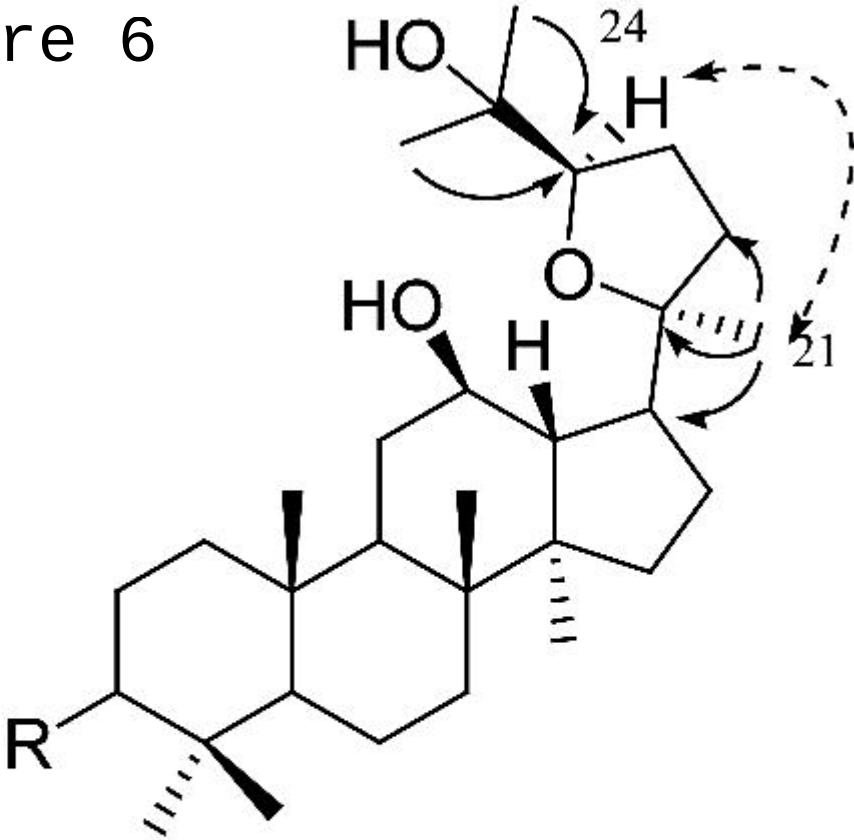

2: R = βOH **4:** R = =O

3: R = βOH **5:** R = =O

HMBC (H → C)

NOESY

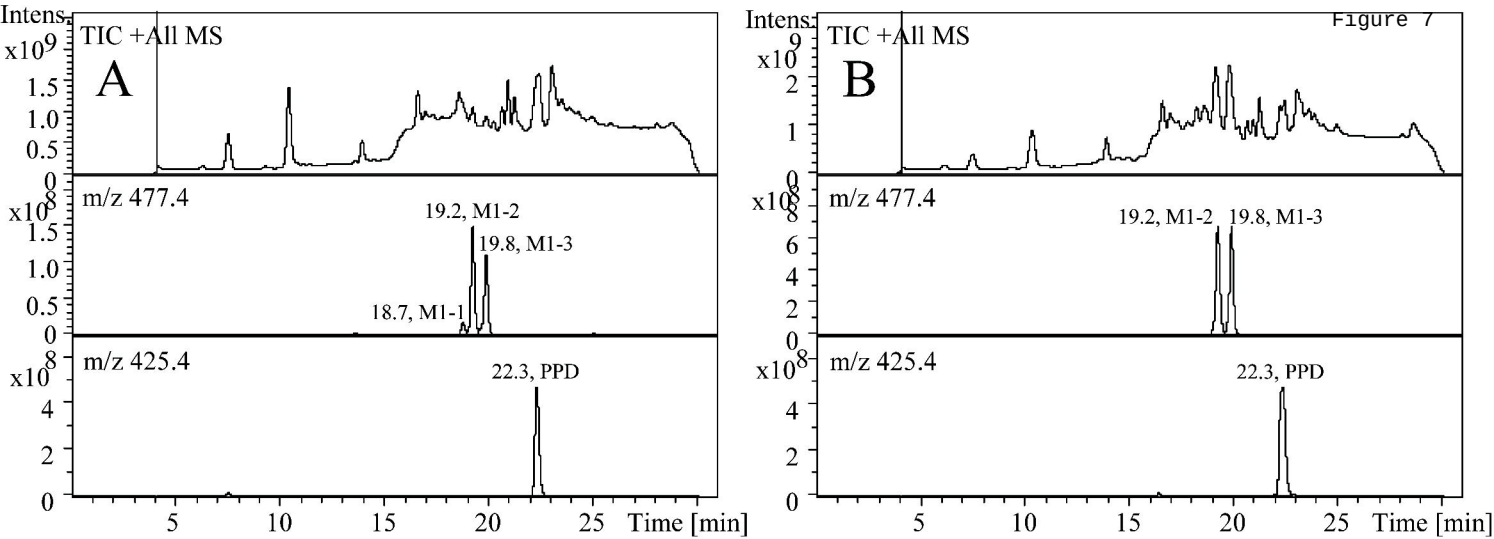
Intens.
TIC +All MS
A
x10 9
1.5
1.0
0.5
0
m/z 477.4
x10 8
19.2, M1-2
19.8, M1-3
18.7, M1-1
m/z 425.4
22.3, PPD
5
10
15
20
25
Time [min]
Intens.
TIC +All MS
B
Figure 7
m/z 477.4
19.2, M1-2
19.8, M1-3
m/z 425.4
22.3, PPD
Time [min]

Figure 8

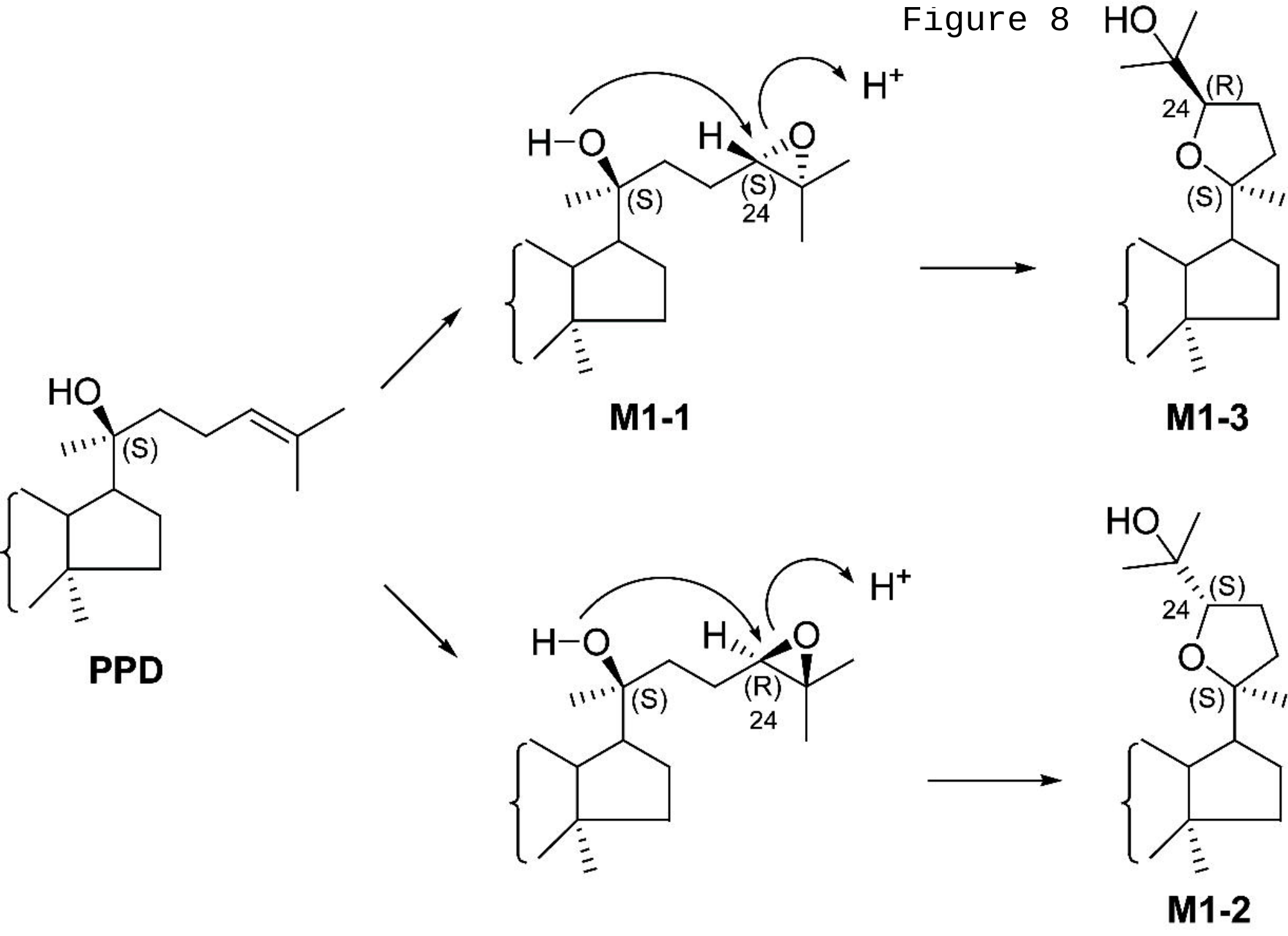

DMD Fast Forward. Published on December 7, 2010 as DOI: 10.1124/dmd.110.036723
This article has not been copyedited and formatted. The final version may differ from this version.